RSC Advances

ROYAL SOCIETY OF CHEMISTRY

www.rsc.org/advances

Graphical Abstract

A new mononuclear coumarin derived Zn(II) complex was design and synthesized and its interaction with DNA and protein was carried out.

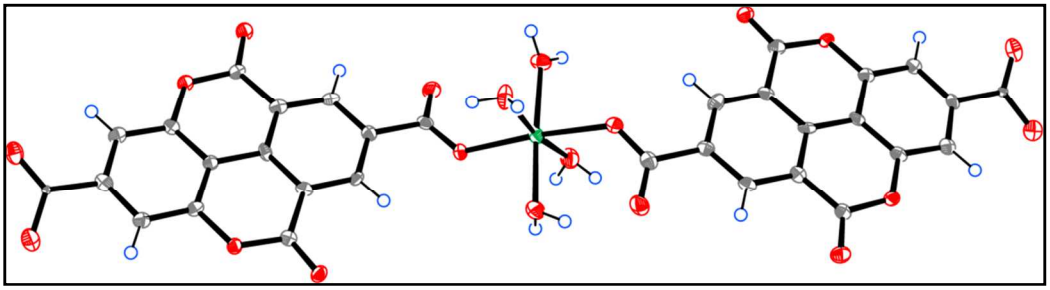

Synthesis, structure elucidation and DFT studies of a new coumarin derived Zn(II) complex: *In vitro* DNA/HSA binding profile and pBR322 cleavage pathway

Ruchi Singh[a], Mohd. Afzal[b], Mehvash Zaki[b], Musheer Ahmad[a], and Sartaj Tabassum[b*]

[a]*Department of Chemistry, Indian Institute of Technology Kanpur, UP–208016, India*
[b]*Department of Chemistry, Aligarh Muslim University, Aligarh, UP–202002, India.*
** Corresponding author:*
Aligarh Muslim University, Aligarh, UP–202002, India.
Tel.: +91 9358255791
E–mail address: tsartaj62@yahoo.com (S. Tabassum)

Abstract

A new mononuclear zinc complex **1** bearing bioactive coumarin scaffold 5,10–dioxo–5,10–dihydro–chromeno[5,4,3–cde]chromene–2,7–dicarboxylic acid was synthesized and characterized by elemental analysis and spectroscopic techniques and further validated by single X–ray crystallography. The DFT studies were performed using *ab initio* Gaussian 09 software package with B3LYP/6–31+g(d,p) basis function. The *in vitro* DNA binding studies of complex **1** with calf–thymus DNA in Tris–HCl buffer was studied by various biophysical techniques which reveal that **1** binds to CT DNA non–covalently *via* electrostatic interactions. Competitive binding experiments showed that **1** has the ability to displace DNA–bound EB. Compound **1** exhibits efficient photoinduced DNA cleavage with supercoiled pBR322 involving hydrolytic cleavage pathway due to the presence of coordinated water molecules. Such synthetic hydrolytic nucleases are gaining considerable attention owing to their importance in biotechnology and drug design, in particular to cleave DNA with sequence selectivity different from that of the natural enzymes.

Introduction

Coumarins (both natural and synthetic) and their analogues are the key components of many bioactive compounds. *In lieu* of broad spectrum of biological activities exhibited by coumarin and its derivatives such as anticancer,[1] antioxidant,[2] anti–inflammatory,[3] anti–HIV,[4] antimicrobial,[5] and anticoagulant[6] they are highly in demand for use as precursors in metal–based drug regime. These compounds serve as unique, versatile scaffolds for the development of newer drugs which may exhibit mechanism of action *via* diverse biological targets for the development of therapeutic agents.[7] Many biologically active compounds used as drugs possess modified pharmacological and toxicological potentials when administered in the form of metal–based compounds.[8] Zinc, an endogenously biocompatible metal ion exists as a divalent cation in the biological system and it is actively involved in DNA synthesis, apoptosis, gene expression, and catalytic functions.[9] Zinc complexes with diverse biological activity *viz*. antibacterial,[10] anti–inflammatory,[11] treatment of Alzheimer disease[12] and anti–proliferative, antitumor[13] activity have been reported. Besides this, Zn(II) complexes are regarded as one of the best suited metal ion for the development of artificial metallonucleases owing to the strong Lewis acidity, vary rapid ligand exchange ability, low toxicity, redox inertness, catalyzing of hydrolytic cleavage of DNA.[14]

Since DNA is the primary intracellular target of anti–cancer drugs, the interaction between small molecules and DNA can cause DNA damage in cancer cells, blocking the division of cancer cells, and resulting in cell death.[15] Small molecules can interact with DNA through the following three non–covalent modes: intercalation, groove binding, and external static electronic effects. Recently, there has been great interest on the binding of metal–based small molecular entities that are more suited for DNA binding, because of their cationic character and three–

dimensional structural profiles, have a natural aptitude to interact with DNA and may give rise to cleaving reactions which is crucial for the development of new cancer therapeutic agents.[16] Similarly, the interaction of metallo–drugs with human serum albumin is of great concern to understand the drug absorption, transport and distribution in the body system in order to modulate their delivery to cells at specific sites. Serum protein binding can lead to premature decomposition of a metal–based agent through ligand exchange.[17]

Herein, we describe the synthesis, spectroscopic characterization and single crystal X–ray studies of the Zn(II) complex (**1**) of the *in situ* generated chromone scaffold; 5,10–dioxo–5,10–dihydro–chromeno[5,4,3–cde]chromene–2,7–dicarboxylic acid (**H_2L**). *In vitro* DNA binding profile of **1** with CT–DNA was carried out by employing UV–vis, fluorescence and circular dichroic techniques in order to demonstrate their affinity towards the molecular drug target DNA. The Photo–induced DNA cleavage studies of **1** on irradiation with monochromatic UV–A light of 365 nm with pBR322 DNA was performed at different concentration and further investigations have also been carried out in the presence of radical scavengers, to clarify the mechanistic pathway. Furthermore, the interaction of **1** with human serum albumin (HSA) was investigated in order to understand the drug-protein interaction and the carrier role of HSA in the drug transportation under physiological condition in Tris–HCl buffer solution at pH 7.4 by employing fluorescence quenching method.

Results and discussion

Compound **1** has been synthesized and characterized by analytical and spectral studies. The formulation of the complex was confirmed by single–crystal X–ray diffraction and further supported by thermo–gravimetric analysis (TGA) and elemental analysis, while the phase purity

of the bulk material is confirmed by powder X–ray diffraction (PXRD). Once isolated, it is found to be air–stable and soluble in DMSO.

Crystal Structure Description

The complex **1** is synthesized by the solvothermal reaction of biphenyl–2,4,6,2',4',6'–hexacarboxylic acid with $Zn(NO_3)_2 \cdot 6H_2O$ in mixed *N,N'*–dimethylformamide and water solvent at 100 °C for 3 days to afford orange block shaped crystals. Single crystal X–ray structural study reveals that **1** crystallizes in the monoclinic space group $P2_1$. The asymmetric unit consists of one Zn(II) ion, two HL^- ligand moieties and four coordinated water molecules (Fig. 1). The coordination environment around Zn(II) ion can be portrayed as a slightly distorted octahedral geometry with ligation from carboxylate group of two ligand moieties in a monodentate fashion (Zn–O = 2.064(4) – 2.101(4)) and four coordinated aqua molecules (Zn–Ow = 2.075(5) – 2.121(4)). The Zn–O bond distances are within the range reported for other Zn based octahedral complexes.[18] Here, both the carboxylate and carbonyl oxygen atoms of the ligand form extensive H–bonding with the coordinated aqua molecules (–C=O···OW=2.073−2.215Å, COOH···OW=1.913−2.325Å). Aromatic rings in translationally equivalent molecules lie in parallel planes and are involved in face–to–face π–π stacking interactions at a ring centroid distance of ~3.39 Å (Fig. 2).[19] These non–covalent interactions result in an overall 3D supramolecular architecture.

Theoretical Calculations

In order to gain some insight into molecular geometry we have performed quantum mechanical calculation of the free molecule. In Table S1, selected geometrical parameters from single crystal X–ray structure are in excellent agreement with those obtained from first–principle density functional (DFT) calculations on complex **1**. The optimized lattice parameters are a =

11.548 Å, b =5.326 Å, c = 23.007 Å, α=γ=90°, and β= 100.3°, which compare well with the experimental crystal parameters. The optimized structure shows a significantly large resemblance with the X–ray crystal structure as depicted in Fig. 3. The Mulliken spin density on the metal centre is found to be zero. This is consistent with the +2 oxidation state of zinc (d^{10}). HOMO is localised on carboxylate groups of the ligand and metal centre while the LUMO is located on the metal centre. This distribution of electron density in the HOMO and LUMO (Fig. 4), implies that during an absorption process, the charge is shifted from HOMO to LUMO. Hence, the electron density change between ligand and metal centre is ascribed to LMCT process.

Thermal and Powder X–ray studies

In order to examine the thermal stabilities of complex **1**, thermal analysis was carried out in a N_2 atmosphere at the rate of 5 °C per minute. Complex **1** shows a weight loss of ~9.25% (expected = 9.15%) within the temperature range 70–120 °C that corresponds to the release of four coordinated water molecules. Decomposition of the complex is achieved beyond 250 °C (Fig. S1). A powder X–ray diffraction (PXRD) pattern of **1** match well with the simulated patterns obtained from the single crystal X–ray data confirming the crystals are truly representative of the bulk phase (Fig. S2). The differences in intensity could be due to the different orientation of the powder sample.

DNA binding studies

The DNA–binding metal complexes have been extensively studied as DNA structural probes, DNA footprinting and sequence–specific cleaving agents and potential anticancer drugs. Many compounds exert their antitumor effects through binding to DNA thereby changing the replication of DNA and inhibiting the growth of the tumor cells, which is the basis of designing

new and more efficient antitumor drugs and their effectiveness depends on the mode and binding affinity.[20–22]

Electronic absorption spectroscopy is one of the most frequently used techniques for the investigation of the binding mode of small molecules to DNA. For **1**, we could anticipate different binding modes on the basis of structure, functional ligand and metal ions, *viz*.: groove binding, coordinate covalent linkage with nucleobase due to Zn(II) metal ion. Besides, chromophore of coumarin ligand could facilitate hydrophobic and H–bonding interactions. Upon addition of increasing amounts of CT–DNA to fixed concentration of **1** in 5 mM Tris–HCl, 50 mM NaCl, pH 7.3 buffer, there is an increase in the absorption intensity of the intraligand absorption band. These spectral features (hyperchromism) indicate minor groove binding, unwinding of DNA double helix, simultaneous exposure of the DNA bases, and damage to the DNA double helix (Fig. 5).[23] The results reveal that the complex interacts with DNA either by external contact (electrostatic interaction) with the phosphate backbone of DNA double helix or the carbonyl and carboxylate groups in **1** can form H–bonds with suitable donors like N3 of adjacent thymine base of DNA, supported by the favorable hydrophobic interaction of coumarin ring on the surface of DNA, contributing to the overall hyperchromism. The intrinsic binding constant K_b for **1** is calculated from the plot of [DNA]/(ε_a–ε_f) versus [DNA] and is found to be 5.12×10^4 M^{-1}. The K_b value of the complex is smaller than those observed for classical intercalators (e.g. ethidium bromide (EB) and $[Ru(phen)_2 (dppz)]_2^{2+}$~$10^6$–$10^7 M^{-1}$) and similar to those of the corresponding Zn(II) complexes reported previously by our group.[24]

Complex **1** exhibits emission at 331 and 360 nm in 0.01Tris–HCl/50 mM NaCl buffer when excited at 267 nm. Upon addition of increasing amount of CT–DNA (0–0.66) $\times 10^{-5}$ M, to fixed amount of **1**, the emission intensity of both peaks increases (Fig. 6), indicating that **1**

interacts with DNA. This is due to the fact that hydrophobic environment inside the DNA helix reduces accessibility of the solvent molecules and restricts its mobility at the binding site which causes reduction of the vibrational modes leading to higher emission intensity.[25] To determine the interacting strength of **1**, binding constant (*K*) value determined from Scatchard equation for complex **1** was found to be 5.37 x 10^4 M^{-1} consistent with electronic absorption studies. To further investigate the interaction of **1** with the DNA, three−dimensional (3D) fluorescence spectroscopy was performed on **1** in the absence and presence of CT−DNA. As depicted in Fig. 7, two prominent peaks, peak A and peak B at λ_{em} = 333 and 369 nm respectively are observed upon excitation at 270 nm. However, addition of DNA leads to significant increase of the fluorescence intensity due to interaction of **1** with DNA.

Competitive ethidium bromide displacement assay is carried out to investigate interaction of **1** with DNA. EB is a planar cationic dye that is widely used as a sensitive fluorescence probe and emits intense fluorescence in the presence of DNA due to its strong intercalation ability between the adjacent DNA base pairs.[26] Upon addition of **1** to the EB–DNA system, appreciable reduction in the fluorescence intensity of about 84% (603 nm) with blue shift is observed either by replacing the DNA–bound EB or by accepting an excited state electron from EB possibly deforming the secondary structure of DNA (Fig. 8).[27] Since EB is not completely displaced, intercalative mode of binding in addition to the electrostatic interaction cannot be ruled out. The quenching efficiency K_{sv} evaluated from the slope of I_0/I *vs* r =[complex]/[DNA] is found to be 0.42.

To assess conformational changes in the DNA and complex **1**, circular dichroism (CD) experiments are carried out. The CD spectra of CT–DNA exhibit a positive band at 275 nm (+ 0.51 mdeg) due to the base stacking and a negative band at 245 nm (–0.60 mdeg) due to the

helicity, which is characteristic of chiral B–DNA molecule. Upon addition of **1**, the CD spectra show only a slight change in the ellipticity for both positive and negative bands revealing that the double helical structure is only slightly perturbed (Fig. 9). The results reveal that both positive band at 274 nm (+0.28 mdeg) and negative band at 237 nm (–0.55 mdeg) display a decrease in the ellipticity and a slight blue–shift in the maximum wavelengths indicating conformational conversion from B→Z helix, together with increased winding of the DNA helix through the rotation of the bases.

HSA binding studies

Fluorescence quenching mechanism

The emission quenching experiment is carried out to study the interaction of complex **1** with HSA (Fig. 10). The HSA shows maximum emission wavelength at 327 nm mainly due to the tryptophan residue.[28] Molecules that bind to albumin particularly in the region containing this Trp residue can cause fluorescence quenching of albumin when excited at 295 nm. The fluorescence spectra of HSA in the absence and presence of **1** as a quencher in Tris–HCl buffer (pH 7.4) is monitored with an excitation wavelength of 295 nm. On addition of increasing concentration of **1** (0.67×10^{-5} to 4.6×10^{-5} M) to fixed amount of HSA, intrinsic fluorescence intensity of HSA decreased gradually at 327 nm up to 86% accompanied by a slight blue–shift of 2 nm in the tryptophan emission maxima of HSA. The observed blue–shift is mainly due to the decrease in the polarity or an increase in the hydrophobicity of the microenvironment surrounding the fluorophore site.[29] These results indicate that the strong protein–binding ability of complex **1** leads to changes in protein secondary structure (affecting the tryptophan residues of HSA) together with enhanced hydrophobicity.[30]

In order to speculate the possible fluorescence quenching mechanism of HSA in presence of **1,** Stern–Volmer equation is applied:

$$\frac{F_o}{F} = 1 + K_q \tau_o [Q] = 1 + K_{sv}[Q] \quad (1)$$

where F_o and F are the fluorescence intensities in the absence and presence of quencher, respectively, K_q, K_{sv}, τ_o and [Q] are the quenching rate constant of the biomolecules, the Stern–Volmer quenching constant, the average life–time of the molecule without quencher ($\tau_o = 10^{-8}$ s) and the concentration of the quencher, respectively. The Stern–Volmer plots of F_o/F versus [Q] for the quenching of HSA fluorescence by **1** is depicted in Fig. S3a and the calculated K_{SV} and K_q values are found to be 3.24×10^3 M^{-1} and 3.24×10^{12} $M^{-1}s^{-1}$ respectively. The observed K_q value is larger than the limiting diffusion constant K_{dif} of the biomolecules ($K_{dif} = 2.0\times10^{10}$ $M^{-1}s^{-1}$),[31] indicating that the fluorescence quenching is mainly due to the specific interaction of **1** with HSA, consistent with the static quenching mechanism.[32] For static quenching, the Scatchard equation is employed to calculate the binding constant and number of binding sites:[33]

$$\log\left[\frac{F_o - F}{F}\right] = \log K + n \log[Q] \quad (2)$$

where F_o and F are the fluorescence intensities of HSA in the absence and presence of quencher, K and n are the binding constant and the number of binding sites, respectively. Thus, a plot of $\log[(F_o–F)/F]$ versus log[Q] is used to determine *K* (binding constant) from the intercept on Y–axis and *n* (binding sites) from the slope (Fig. S3b). From the corresponding Scatchard plot, the K and n values for **1** is calculated to be 0.526 and 1.06 respectively. The calculated K value of **1** is lower than the association constant of one of the strongest known non–covalent bonds of avidin–ligands interaction ($K \approx 10^{15}$ M^{-1}) suggesting a possible release from the serum albumin to the targeted cells.[34]

In order to further gain insight in the conformational changes of proteins, 3D fluorescence spectral studies are carried out in the presence and absence of complex **1**. The 3D fluorescence spectra and contour ones of HSA and complex **1**–HSA system are shown in Fig. 11, respectively. Peak A is the Rayleigh scattering peak ($\lambda_{ex} = \lambda_{em}$). Peak B ($\lambda_{ex}$ = 295, λ_{em} = 332 nm) dominatingly displays spectral behavior of the Trp residue, and the fluorescence intensity of this residue is associated with the micro–environment's polarity of HSA. The results reveal that fluorescence intensity of peak **A** increases and that of peak **B** (295, 332 nm, λ_{ex}, λ_{em}) decreases significantly indicating quenching of fluorescence induced by Trp residue of HSA. However, the fluorescence intensity of peak B is strongly quenched revealing that **1** binds to HSA near the tryptophan residues.[35] The results reveal that the interaction of **1** with HSA induced micro–environmental changes in the structure of HSA, corroborated well with our spectroscopic results obtained from UV–vis, and fluorescence measurements.

Photoinduced DNA cleavage activity

The photoinduced DNA cleavage by the small molecules is considered to be most suitable therapeutic agent as they can be photoinduced to give localized action by irradiating the affected area and thereby unwanted DNA damage can be avoided. It is known that DNA cleavage is reflected by relaxation of the supercoiled circular form of pBR322 DNA resulting in nicked circular and/or linear forms. The ability of Zn(II) complexes to mediate DNA cleavage is well established in literature owing to the fact that zinc ion is regarded as one of the best suited metal ion for the development of artificial metallonucleases; catalyzing hydrolytic cleavage of DNA due to its strong Lewis acid and redox inert nature, it is therefore imperative to study the effect of Zn(II) complex of bioactive scaffold on pBR322 DNA in a concentration dependent manner, the presence of reactive oxygen species and DNA recognition elements (groove binding).

The DNA cleavage activity of complex **1** was studied by using pBR322 DNA in 5 mM Tris–HCl/50 mM NaCl buffer (pH 7.3) on irradiation with UV light in the absence of any external additives (Fig. 12). With increasing concentrations (Lanes 20–60 μM) of the complex **1**, the amount of Form I of pBR322 DNA diminishes gradually, whereas Form II increases gradually (Lanes 2–5) without the formation of Form III, suggesting single strand DNA cleavage. However, at 60 μM concentration of **1**, the intensity of both the forms increases apparently (Lane 6) with the maximum intensity of Form II indicating the efficient cleavage activity which may be due to the production of more hydroxyl radical by the presence of aqua ligands leads to DNA hydrolysis. So, we conclude that the cleavage activity was dependent on metal ion concentration and presence of active coumarin moiety which acts as a photosensitizer and could be responsible for the higher photocleavage activity in UV light.[36]

In order to determine the reactive species that are responsible for the photoactivated cleavage of the pBR322 DNA, cleavage experiments were carried out in presence of various additives such as hydroxyl radical scavengers (DMSO, EtOH), singlet oxygen quencher (NaN_3) and a superoxide scavenger (SOD) as shown in Fig. 13. Addition of DMSO and EtOH (hydroxyl radical scavengers) to the reaction mixture exhibit partial inhibition in the DNA photocleavage activity suggesting the formation of hydroxyl radical ($^{\bullet}OH$) as reactive oxygen species (ROS). Singlet oxygen scavengers, *viz*., sodium azide also scarcely inhibited the DNA photocleavage activity. Furthermore, the addition of SOD does not show any effect on the DNA photocleavage activity suggesting non–involvement of peroxide radicals. The results reveal that complex **1** is able to cleave efficiently in presence of hydroxyl radicals as the reactive oxygen species (ROS) responsible for the photo–damage of DNA which implies that DNA might be cleaved by a discernible hydrolytic pathway. Hydrolytic pathways usually depend on the Lewis acidity of the

central metal ion, which serves to activate the phospho–diester bonds towards nucleophilic attack *via* charge neutralization. The present complex contain coordinated water molecule, which facilitates the nucleophilic attack of water oxygen to phosphorus, followed by a five–coordinate phosphate intermediate and subsequent rearrangement of the phosphate allows the DNA to be cleaved readily.

The DNA groove binding propensity of the complexes is explored by using complex **1** and minor groove binder DAPI and major groove binder methyl green (MG). Significant inhibition of DNA cleavage by **1** in the presence of DAPI indicates the binding of the complex to DNA through the minor groove.

Conclusion

In this work, we have designed and synthesized a new zinc(II) molecular entity (**1**) possessing pharmacologically active chromone scaffold; 5,10–dioxo–5,10–dihydro–chromeno[5,4,3–cde]chromene–2,7–dicarboxylic acid (**H_2L**) and thoroughly characterized by elemental and spectroscopic techniques in accordance with single X–ray crystallography. The DFT studies was performed by using *ab initio* electronic structure program Jaguar (B3LYP method) and the HOMO–LUMO gap of 0.238 eV indicates the high stability of this molecule. The *in vitro* DNA binding studies of complex **1** was carried out to examine its effect on DNA binding propensity which reveals an electrostatic mode of binding, in addition to selective recognition towards the minor groove of DNA. The complex **1** cleaves supercoiled plasmid pBR322 DNA through hydrolytic mechanism. Furthermore, affinity of complex **1** for HSA was investigated in order to understand the carrier role of serum albumin for complex **1** in blood under physiological conditions which demonstrated that complex **1** binds with HSA with low affinity as compared to DNA, suggesting a possible release from the serum albumin to the DNA in the targeted cells.

Experimental

Materials

Reagent grade 2–bromo–1,3,5–trimethyl–benzene and $Zn(NO_3)_2 \cdot 6H_2O$ were procured from Aldrich and Calf thymus DNA (CT DNA), 6X loading dye (Fermental Life Science) and Supercoiled plasmid DNA pBR322 (Genei) were used as received. HSA (fatty acid free, 99%) was purchased from Sigma and used without further purification.

Methods and instrumentation

Carbon, hydrogen and nitrogen contents were determined on Elementar Vario EL III model. Molar conductance was measured at room temperature on CON 510 Bench conductivity TDS Meter. IR spectrum was recorded on Interspec 2020 FTIR spectrometer in KBr pellets from 400–4000 cm^{-1}. The NMR spectra were obtained on a Bruker DRX–400 spectrometer operating at room temperature. Electrospray mass spectra were recorded on Micromass Quattro II mass spectrometer. XRD were recorded on Rikagu mini Flex II Instrument. The EPR spectrum of the copper complex was acquired on a Varian E 112 ESR spectrometer using X–band frequency (9.5 GHz) at liquid nitrogen temperature in liquid state. Electronic spectrum was recorded on UV–1700 PharmaSpec UV–vis spectrophotometer (Shimadzu) in DMSO cuvettes of 1 cm path length. Data were reported in λmax/nm. Fluorescence measurements were determined on a RF–5301 PC spectrofluorophotometer (Schimadzu).

Synthesis of Ligand

The ligand was synthesized in the following steps.

The precursor biphenyl–2,4,6,2',4',6'–hexacarboxylic acid was synthesized with slight modifications (Scheme 1), following an earlier reported procedure[37].

(1) Synthesis of trimethyl 2–bromobenzene–1,3,5–tricarboxylate (Triester)

To a stirred mixture of 2–bromomesitylene (5.0 g, 0.025 mol) and aqueous NaOH (1.3 g, 0.0325 mol, 50 ml H_2O) under reflux, solid $KMnO_4$ (26.4 g, 0.167 mol) was added in portions during a period of 4 h. After additional 4 h heating, the excess of $KMnO_4$ was destroyed by addition of 25 ml methanol. The mixture was filtered and the separated MnO_2 was washed with hot water. The filtrate and washings were combined, concentrated to 30 ml and acidified to ~pH 1 with concentrated HCl. The deposited triacid was isolated by filtration, washed with water and dried. Yield: 3.25 g (65.0%). Melting point: 291–294 °C. The crude acid (2.0 g, 6.92 mmol) was suspended in methanol (60 ml), concentrated sulfuric acid (5 ml) was added and the mixture was heated to reflux overnight. The volume was reduced and poured in ice–cold water whereby a white precipitate was obtained which was filtered, washed with water and dried. Yield 1.72 g (86.0%). Melting Point: 93–95 °C. ^{1}H–NMR (DMSO–d_6, 500 MHz), δ (ppm): 8.62(s, 2H, H_{Ar}), 3.75(s, 9H, CH_3). ^{13}C–NMR (DMSO–d_6, 125 MHz), δ (ppm): 167.8, 149.8, 129.9, 129.4, 127.9, 55.2. ESI–MS: m/z [M+1] 332.1071(100%). Elemental analysis: Calcd. for $C_{12}H_{11}BrO_6$: C, 43.53; H, 3.35%; Found: C, 43.65; H, 3.21% (Figs. S4–S6).

(2) Synthesis of 1,1′–biphenyl–2,2′,4,4′,6,6′–hexacarboxylic Acid (H_6L)

Trimethyl 2–bromobenzene–1,3,5–tricarboxylate (1.7 g, 0.005 mol) was taken in round bottomed flask containing dry xylene (40 mL) provided with a reflux condenser and a thermometer. The mixture was refluxed with vigorous stirring under argon atmosphere for 20 min. Copper powder (0.41 g, 0.006 mol) was added to the stirred mixture. The mixture was refluxed for another 90 min. After that, a second portion of copper powder (0.21 g) was added, continued to reflux for an additional hour. The solution was filterd hot and washed extensively with dichloromethane to afford a white colored filtrate. Complete removal of solvent under reduced pressure affords 1.4 g of crude product as a pale yellow powder. The crude product was recrystallized from methanol. This hexaester (1.2 g, 0.002 mol) was hydrolyzed by refluxing it

with 6N NaOH solution (20 mL) for 24 h. After cooling to 5° C, the resulting solution was acidified with 6N HCl solution to obtain a white precipitate. It was collected by filtration, washed thoroughly with water and dried in air. Yield: 1.02 g (85 %). Melting point > 370 °C. ^{1}H–NMR (DMSO–d_6, 500 MHz), δ (ppm): 8.67 (s, 4H; H_{Ar}). ^{13}C–NMR (DMSO–d_6, 125 MHz), δ (ppm): 170.1, 167.0, 147.8, 138.9, 132.3, 129.8. ESI–MS: m/z [M−1] 416.9977(100%). Elemental analysis: Calcd. for $C_{18}H_{10}O_{12}$: C, 51.69; H, 2.41%. Found: C, 51.48; H, 2.34% (Figs. S7–S9).

(3) Synthesis of $[Zn(HL)_2\cdot(H_2O)_4]$ (1)

The ligand 5,10–dioxo–5,10–dihydro–chromeno[5,4,3–cde]chromene–2,7–dicarboxylic acid (**H_2L**) was achieved *via in situ* solvothermal synthesis. To the best of our knowledge, this is the first example wherein a chromene moiety is generated *in situ* by solvothermal synthesis. Biphenyl–2,4,6,2',4',6'–hexacarboxylic acid (40 mg, 0.096 mmol), $Zn(NO_3)_2\cdot 6H_2O$ (60 mg, 0.19 mmol), 2mL of DMF and 1mL of H_2O were sealed in a Teflon lined autoclave and heated under autogenous pressure to 100°C for three days and then allowed to cool to room temperature at the rate of 1°C per minute. Block shaped orange crystals of **1** were collected in ~54% yield. Melting point 248 °C. Anal. calcd. for $C_{32}H_{18}O_{20}Zn$: C, 48.79; H, 2.30%. Found: C, 48.71; H, 2.39%. IR (cm^{-1}): 3384(s), 1607(s), 1422(s), 1376(s), 1340(m), 1205(m), 940(m), 802(m), 776(s), 720(s). ESI–MS: *m/z* (100%) 788.83 $[M+1]^+$ (Figs. S10 and S11).

Single–crystal X–ray Studies

Single crystal X–ray data of complex **1** was collected at 100K on a Bruker SMART APEX CCD diffractometer using graphite monochromated MoK_α radiation (λ= 0.71073 Å). The linear absorption coefficients, scattering factors for the atoms and the anomalous dispersion corrections were referred from the International Tables for X–ray Crystallography.[38] The data integration and

reduction were worked out with SAINT [39] software. Empirical absorption correction was applied to the collected reflections with SADABS,[40] and the space group was determined using XPREP.[41] The structure was solved by the direct methods using SHELXTL–97[42] and refined on F^2 by full–matrix least–squares using the SHELXTL–97 programme[43] package. Only a few H atoms could be located in the difference Fourier maps in the structure. The rest were placed at calculated positions using idealized geometries (riding model) and assigned fixed isotropic displacement parameters. All non–H atoms were refined anisotropically. Atoms C16 and C32 were refined isotropically. Several DFIX commands were used for fixing some bond distances in complex **1**.The crystal and refinement data are collected in Table 1. Selective bond distances and angles are given in Table S2.

Theoretical Calculations

Quantum chemical calculations were pursued at the level of density functional theory (DFT) to calculate the optimized geometry. Gaussian 09 software package was used to find the optimized energies, energy of frontier molecular orbitals (HOMO and LUMO) with B3LYP/6–31+g(d,p) basis function.[44] Optimizations were carried out employing X–ray coordinates using Becke's three parameter hybrid exchange functional with the Lee–Yang–Parr correlation function (B3LYP).[45–47] Hay and wadt basis set LANL2DZ was used for zinc metal centre while for rest of the atoms 6–31G basis set was employed. Tight convergence criteria were used with the self–consistent field "tight" option in all calculations, in order to ensure sufficiently well convergence. The authenticity of the final optimized geometry was confirmed by the absence of any imaginary frequency values, and also the convergence in force and maximum displacement further established the occurrence of ground state minima.

DNA binding and cleavage experiments

DNA binding experiments include absorption spectral traces, emission spectroscopy and viscosity conformed to the standard methods and practices previously adopted by our laboratory.[48–51] While measuring the absorption spectra an equal amount of DNA was added to both the compound solution and the reference solution to eliminate the absorbance of the CT DNA itself, and Tris buffer was subtracted through base line correction.

HSA binding studies: Sample preparation

Human Serum Albumin of 1×10^{-3} M was prepared by dissolving protein in Tris–HCl buffer solution at pH 7.4. The protein concentration was determined spectrophotometrically using an extinction coefficient of 35219 $M^{-1}cm^{-1}$ at 280 nm.[52] Stock solution of complex (1×10^{-3} M) was prepared by dissolving complex in doubly distilled water. NaCl (analytical grade, 1 M) solution was used to maintain the ionic strength of buffer at 0.1 M pH was adjusted to 7.4 by using HCl. Working standard solution was obtained by appropriate dilution of the stock solution.

Acknowledgements

We gratefully acknowledge the financial support received from the DST–PURSE programme and DRS–1 (SAP) from UGC, New Delhi, India and M. Z is thankful for SRF from CSIR India. PKB gratefully acknowledge the financial support received from the DST–SERB program.

References

[1] F. Belluti, G. Fontana, L. Dal Bo, N. Carenini, C. Giommarelli and F. Zunino, *Bio–organic & Medicinal Chemistry*, 2010, **18**, 3543.

[2] R. S. Hoult and M. Paya, *Gen. Pharmacol*., 1996, **27**, 713.

[3] H. A. Stefani, K. Gueogjan, F. Manarin, S. H. P. Farsky, J. Zukerman–Schpector, I. Caracelli, S. R. P. Rodrigues, M. N. Muscara, S. A. Teixeira, J. R. Santin, I. D. Machado, S. M. Bolonheis, R. Curi and M. A. Vinolo, *Eur. J. Med. Chem*., 2012, **58**, 117.

[4] Y. Kashman, K. R. Gustafson, R. W. Fuller, J. H. Cardellina, J. B. McMahon, M. J. Currens, R. W. Buckheit, S. H. Hughes, G. M. Cragg and M. R. Boyd, *J. Med. Chem*., 1992, **35**, 2739.

[5] M. Basanagouda, K. Shivashankar, M. V. Kulkarni, V. P. Rasal, H. Patel, S. S. Mutha and A. A. Mohite, *Eur. J. Med. Chem*., 2010, **45**, 1151.

[6] R. Deng, J. Wu and L. Long, *Bull. Soc. Chim. Bell* 1992, **101**, 439.

[7] M. J. Matos, C. Teran, Y. Perez–Castillo, E. Uriarte, L. Santana and D. Vina, *J. Med. Chem*. 2011, **54**, 7127.

[8] (a) L. J. Ming, *Med. Res. Rev*. 2003, 23, 697. (b) A. R Timerbaev, C. G Hartinger, S. S Aleksenko and B. K. Keppler, *Chem. Rev*., 2006, **106**, 2224.

[9] G. K. Walkup, S. C. Burdette, S. J. Lippard and R. Y. Tsien, *J. Am. Chem. Soc*., 2000, **122**, 5644.

[10] L. Ze–Quan, W. Feng–Jing, G. Yun, H. Chang–Wen, Z. Yun–Huai and G. Meng–Yu, *Chin. J. Chem*., 2007, **25**, 1809.

[11] Q. Zhou, T. W. Hambley, B. J. Kennedy, P. A. Lay, P. Turner, B. Warwick, J. R. Biffin and H. L. Regtop, *Inorg. Chem.,* 2000, **39**, 3742.

[12] M. D. Vaira, C. Bazzicalupi, P. Orioli, L. Messori, B. Bruni and P. Zatta, *Inorg.Chem*., 2004 **43**, 3795.

[13] D. Kovala–Demertzi, P. N. Yadav, J. Wiecek, S. Skoulika, T. Varadinova and M. A. Demertzis, *J. Inorg. Biochem*. 2006, **100**, 1558.

[14] C. Bazzicalupi, A. Bencini, C. Bonaccini, C. Giorgi, P. Gratteri, S. Moro, M. Palumbo, A. Simionato, J. Sgrignani, C. Sissi and B. Valtancoli, *Inorg. Chem*., 2008, **47**, 5473.

[15] (a) G. Zuber, J. C. Quada Jr. and S. M. Hecht, *J. Am. Chem. Soc*., 1998, **120**, 9368; (b) S. M. Hecht, *J. Nat. Prod*., 2000, **63**, 158.

[16] P. Kalaivani, R. Prabhakaran, F. Dallemer, P. Poornima, E. Vaishnavi, E. Ramachandran, V. V. Padma, R. Renganathan and K. Natarajan, *Metallomics*, 2012, **4**, 101.

[17] A. Tarushi, C. P. Raptopoulou, V. Psycharis, A. Terzis, G. Psomas and D. P. Kessissoglou, *Bioorganic & Medicinal Chemistry*, 2010, **18**, 2678.

[18] R. Singh, M. Ahmad and P. K. Bharadwaj, *Cryst.Growth Des.,* 2012, **12**, 5025.

[19] C. J. Janiak, *Chem. Soc., Dalton Trans*. 2000, 3885.

[20] A. Tarushi, G. Psomas, C. P. Raptopoulou, V. Psycharis and D. P. Kessissoglou, *Polyhedron*, 2009, **28**, 3272.

[21] A. Tarushi, G. Psomas, C. P. Raptopoulou and D. P. Kessissoglou, *J. Inorg. Biochem*., 2009, **103**, 898.

[22] G. Psomas and D. P. Kessissoglou, *Dalton Trans*., 2013, **42**, 6252.

[23] R. K. Gupta, R. Pandey, G. Sharma, R. Prasad, B. Koch, S. Srikrishna, P. –Z. Li, Q. Xu, and D. S. Pandey, *Inorg. Chem*., 2013, **52**, 3687.

[24] F. Arjmand and S. Parveen, *RSC Advances*, 2012, **2**, 6354.

[25] S. S. Bhat, A. S. Kumbhar, P. Lonnecke and E. H. –Hawkins, *Inorg. Chem*. 2010, **49**, 4843.

[26] F. A. Beckford, M. S. Jr., G. Leblanc, J. Thessing, L. C. L. –Alleyne, A. A. Holder, L. Li and N. P. Seeram, *Dalton Trans*., 2009, 10757.

[27] J. Hernandez–Gil, S. Ferrer, A. Castineiras and F. Lloret, *Inorg. Chem*., **51**, 2012, 9809.

[28] A. Tarushi, J. Kljun, I. Turel, A. A. Pantazaki, G. Psomasa and D. P. Kessissoglou, *New J. Chem*., 2013, **37**, 342.

[29] Y. Lu, Q. Feng, F. Cui, W. Xing, G. Zhang and X. Yao, Bioorg. Med. Chem. Lett., 2010, 20, 6899.

[30] X. –F. Zhang, L. Xie, Y. Liu, J. –F. Xiang, L. Li and Y. –L. Tang, *J. Mol. Struct*., 2008, **888**, 145.

[31] C. –Y. Gao, X. Qiao, Z. –Y. Ma, Z. –G. Wang, J. Lu, J. –L. Tian, J. –Y. Xu and S. –P. Yan, *Dalton Trans*., 2012, **41**, 12220.

[32] G. Zhang, N. Zhao and L. Wang, *J. Lumines*. 2011, **131**, 880.

[33] S. Naveenraj and S. Anandan, *J. Photochem. Photobiol*. *C*, 2013, 14, 53.

[34] O. H. Laitinen, V. P. Hytonen, H. R. Nordlund and M. S. Kuloma, *Cell. Mol. Life Sci*., 2006, **63**, 2992.

[35] J. –Q. Tong, F. –F. Tian, Q. Li, Li –L i Li, C. Xiang, Y. Liu, J. Dai and F. –L. Jiang, *Photochem. Photobiol. Sci*., 2012, **11**, 1868.

[36] (a) N. Kumari, B. K. Maurya, R. K. Koiri, S. K. Trigun, S. Saripella, M. P. Coogan and L. Mishra, *Med. Chem. Commun*., 2011, **2**, 1208. (b) Q. Zou, Y. Fang, Y. Zhao, H. Zhao, Y. Wang, Y. Gu, and F. Wu, *J. Med. Chem*., 2013, **56**, 5288. (c) S. Karthik, N. Puvvada, B. N. P. Kumar, S. Rajput, A. Pathak, M. Mandal, and N. D. P. Singh, *Appl. Mater. Interfaces*., 2013, **5**, 5232.

[37] P. Holy, J. Zavada, J. Zezula, I. Cisarova, J. Podlaha, *Collect. Czech. Chem. Commun.,* 2001, **66**, 820.

[38]. International Tables for X–Ray Crystallography; Kynoch Press: Birmingham, England, 1952; Vol. III.

[39]. SAINT, version 6.02; Bruker AXS: Madison, WI, 1999.

[40]. Sheldrick, G. M. SADABS: Empirical Absorption CorrectionProgram; University of Göttingen: Göttingen, Germany, 1997.

[41]. XPREP, version 5.1; Siemens Industrial Automation Inc.: Madison, WI, 1995.

[42]. Sheldrick, G. M. SHELXTL Reference Manual, version 5.1; Bruker AXS: Madison, WI, 1997.

[43]. Sheldrick, G. M. SHELXL–97: Program for Crystal Structure Refinement; University of Gottingen: Gottingen, Germany, 1997.

[44] M. J. Frisch, G. W. Trucks, H. B. Schlegel, G. E. Scuseria, M. A. Robb, J. R. Cheeseman, G. Scalmani, V. Barone, B. Mennucci, G. A. Petersson, H. Nakatsuji, M. Caricato, X. Li, H. P. Hratchian, A. F. Izmaylov, J. Bloino, G. Zheng, J. L. Sonnenberg, M. Hada, M. Ehara, K. Toyota, R. Fukuda, J. Hasegawa, M. Ishida, T. Nakajima, Y. Honda, O. Kitao, H. Nakai, T. Vreven, J. A., Jr. Montgomery, J. E. Peralta, F. Ogliaro, M. Bearpark, J. J. Heyd, E. Brothers, K. N. Kudin, V. N. Staroverov, R. Kobayashi, J. Normand, K. Raghavachari, A. Rendell, J. C. Burant, S. S. Iyengar, J. Tomasi, M. Cossi, N. Rega, N. J. Millam, M. Klene, J. E. Knox, J. B. Cross, V. Bakken, C. Adamo, J. Jaramillo, R. Gomperts, R. E. Stratmann, O. Yazyev, A. J. Austin, R. Cammi, C. Pomelli, J. W. Ochterski, R. L. Martin, K. Morokuma, V. G. Zakrzewski, G. A. Voth, P. Salvador, J. J. Dannenberg, S. Dapprich, A. D. Daniels, Ö. Farkas, J. B. Foresman, J. V. Ortiz, J. Cioslowski and D. J. Fox, Gaussian 09, revision C.01; Gaussian, Inc.: Wallingford, CT, 2010.

[45] (a) A. D. Becke, *J. Chem. Phys.,* 1993, **98**, 5648. (b) A. D. Becke, *Phys. Chem. Rev. A,* 1988, **38**, 3098.

[46] C. Lee, W. Yang and R. G. Parr, *Phys. Rev. B,* 1988, **37**, 785.

[47] R.G. Parr, W. Yang (eds), Density–Functional Theory of Atoms and Molecules, Oxford University Press, New York, **1989**.

[48] F. Arjmand, S. Parveen, M. Afzal, L. Toupet and T. B. Hadda, *Eur. J. Med. Chem.,* 2012, **49**, 141.

[49] F. Arjmand, F. Sayeed, S. Parveen, S. Tabassum, A. S. Juvekar and S. M. Zingde, *Dalton Trans.*, 2013, **42**, 3390.

[50] F. Arjmand, M. Muddassir, Y. Zaidi and D. Ray, *Med. Chem. Commun*., 2013, **4**, 394.

[51] F. Arjmand, F. Sayeed and M. Muddassir, *J. Photochem. Photobiol. B*, 2011, **103**, 166.

[52] C.N. Pace, F. Vajdos, L. Fee, G. Grimsley and T. Gray, *Prot. Sci*., 1995, **4**, 2411.

Figure and Scheme Captions

Scheme 1. Synthetic route to metal complex **1**.

Scheme 2. Proposed intermediate in the hydrolysis of DNA cleavage promoted by complex **1**.

Fig. 1. Schematic view of **(a)** ORTEP diagram (50% probability) of asymmetric unit in complex **1**.

Fig. 2. Diagrammatic representation of (a) 3D packing (in spacefill model) (b) H–bonding and π ···π interactions in complex **1**.

Fig. 3. The optimized geometrical structure of complex **1**.

Fig. 4. The optimized structures showing (a) HOMO and (b) LUMO Frontier Molecular Orbital for complex **1**.

Fig. 5. Absorption spectra of complex **1** in 5mM Tris HCl/ 50 mM NaCl buffer upon the addition of calf thymus DNA; Inset: Plots of [DNA]/ ε_a–ε_f (m^2 cm)vs [DNA] for the titration of CT DNA with complex ▲, experimental data points; full lines, linear fitting of the data. [complex] = 6.67×10^{-6} M, [DNA] = (0–4.24) × 10^{-5} M. Arrow shows change in intensity with increasing concentration of DNA.

Fig. 6. Emission spectra of complex **1** in Tris–HCl buffer (pH 7.3) in the presence and absence of CT DNA at room temperature. Arrow shows change in intensity with increasing concentration of DNA.

Fig. 7. 3D fluorescence spectrum and corresponding contour diagrams of (a) Complex **1** and (b) complex **1**–DNA system. The concentration of complex is fixed at 1.46 mM and that of DNA is fixed at 11.5 mM.pH = 7.3, at room temperature.

Fig. 8. Emission quenching spectra of CT DNA bound ethidium bromide in the presence of (a)complex **1** in buffer 5 mM Tris–HCl/50 mM NaCl, pH = 7.3 at 25 ºC. Arrow shows change in intensity with increasing concentration of ethidium bromide.

Fig. 9. CD spectra of CT–DNA (blue, 1×10^{-4} M) in the presence of complex **1** (green**,** 1×10^{-4} M), at [complex]/[DNA] molar ratios of 0.03.

Fig. 10. The fluorescence quenching spectra of HSA by different concentrations of complex**1** with the excitation wavelength at 293 nm in 5 mM Tris–HCl/50 mM NaCl buffer, pH 7.4, at room temperature: [HSA], 6.67×10^{-6}M; the concentration of complex **1**was 0.67×10^{-5} to 4.6×10^{-5} M. Arrow shows the intensity changes upon increasing concentration of the quencher.

Fig. 11. 3D fluorescence spectrum and corresponding contour diagrams of (a) HSA, and (b) complex **1**–HSA system. The concentration of HSA is fixed at 1.6 mM and that of complex **1** is fixed at 13.5 mM.pH = 7.4, at room temperature.

Fig. 12. Cleavage of pBR322 plasmid DNA (300ng) by complex **1** in 50 mM Tris–HCl/NaCl buffer (pH, 7.3) on photo–irradiation in monochromatic UV–A1 light of 365 nm after 40 min exposure time at different concentration; Lane 1: DNA control; Lane 2: 20 μM **1** +

DNA; Lane 3: 30 μM **1** + DNA; Lane 4: 40 μM **1** + DNA; Lane 5: 50 μM **1** + DNA; Lane 6: 60 μM **1** + DNA.

Fig. 13. Cleavage of pBR322 plasmid DNA (300ng) by complex **1** in 50 mM Tris–HCl/NaCl buffer (pH, 7.3) on photo–irradiation in monochromatic UV–A1 light of 365 nm after 40 min exposure time in the presence of different scavenging and groove binding agents; Lane 1, DNA control; Lane 2, DNA + **1** + DMSO (0.4 mM); Lane 3, DNA + **1** + EtOH (0.4 mM); Lane 4, DNA + **1** + NaN_3 (0.4 mM); Lane 5, DNA + **1** + SOD (0.25 mM); Lane 6, DNA + **1** + MG (2.5 μL of a 0.01 mg/ml solution); Lane 7, DNA + **1** + DAPI (8 μM)

Table 1. Crystal and Structure Refinement Data for **1.**

Parameters	**1**
formula	$C_{32}H_{18}O_{20}Zn$
Fw (g mol^{-1})	787.83
cyst syst	Monoclinic
space group	*P*21
a (Å)	11.5488(19)
b (Å)	5.3260(9)
c (Å)	23.007(4)
α (deg)	90.00
β (deg)	100.302(3)
γ (deg)	90.00
U ($Å^3$)	1392.3(4)
Z	2
ρ_{calc} (g/cm^3)	1.874
μ (mm^{-1})	0.989
F(000)	796
crystal size (mm)	0.21 × 0.16 × 0.13
Temp (K)	100(2)
measured reflns	7456
unique reflns	4795
θ Range (deg)/ completeness (%)	1.80to 25.50/ 0.989
GOF[a]	1.064
Final R[b] indices	*R*1 = 0.0480

R^b indices	$R1 = 0.0530$
largest diff. peak/hole (e.Å^{-3})	1.141/–0.550

[a]GOF is defined as $\{\sum[w(F_0^2 - F_c^2)]/(n-p)\}^{1/2}$ where n is the number of data and p is the number of parameters. [b]R = $\{\sum \|F_0| - |F_c\| / \sum |F_0|, wR_2 = \{\sum w(F_0^2 - F_c^2)^2 / \sum w(F_0^2)^2\}^{1/2}$

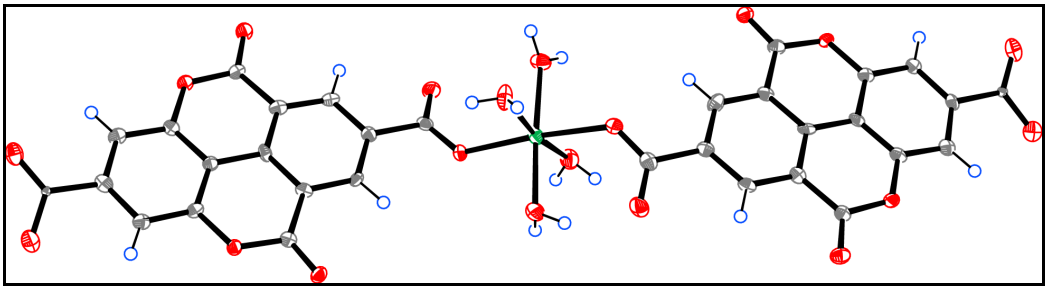

Fig. 1

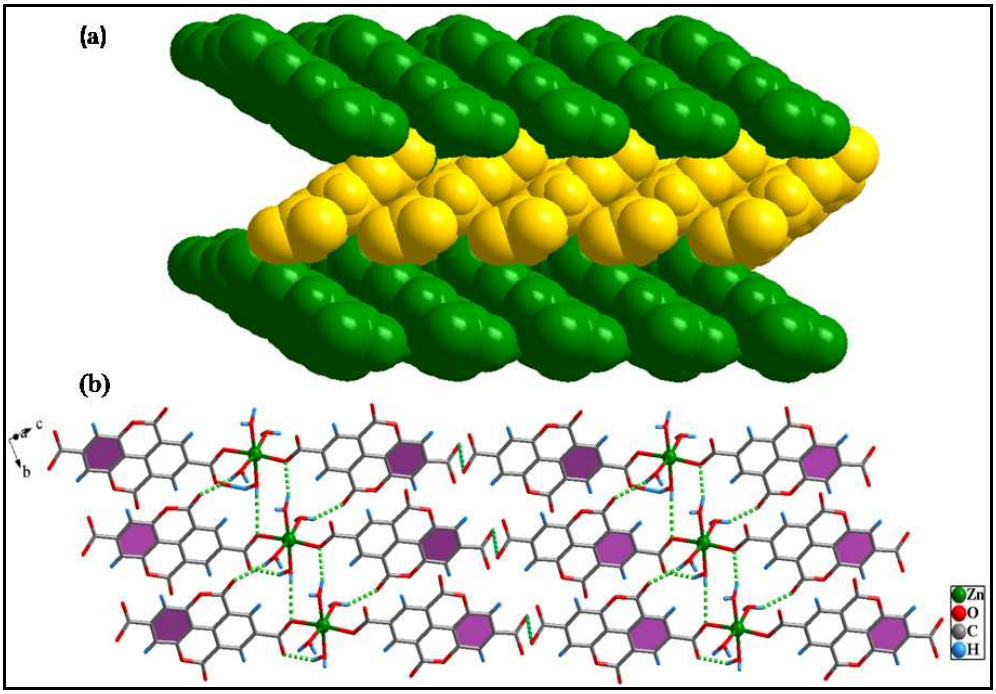

Fig. 2

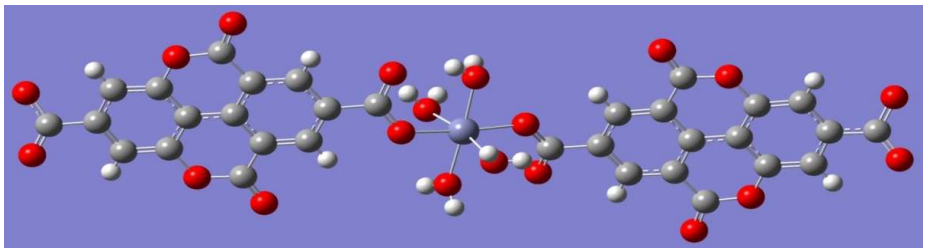

Fig. 3

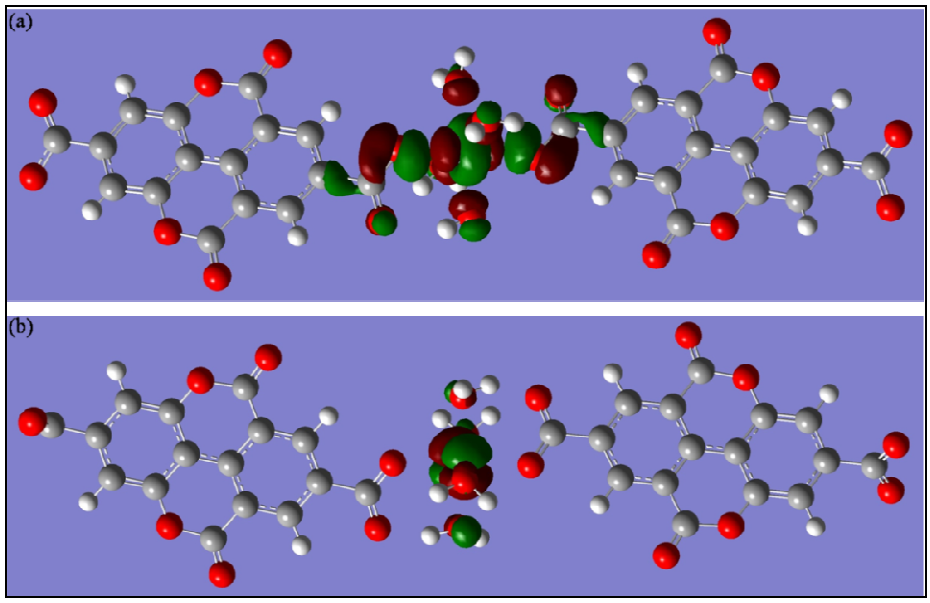

Fig. 4.

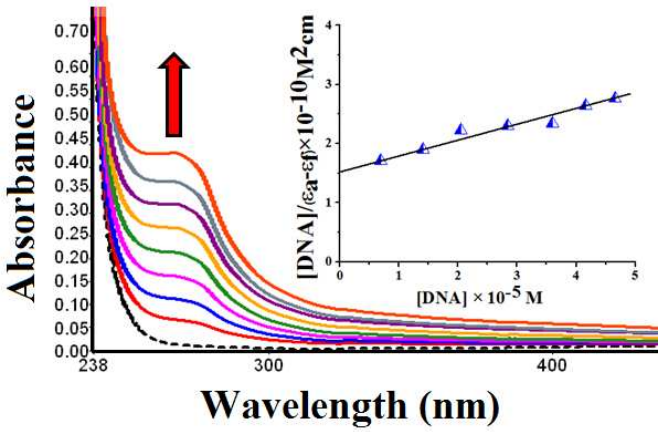

Fig. 5

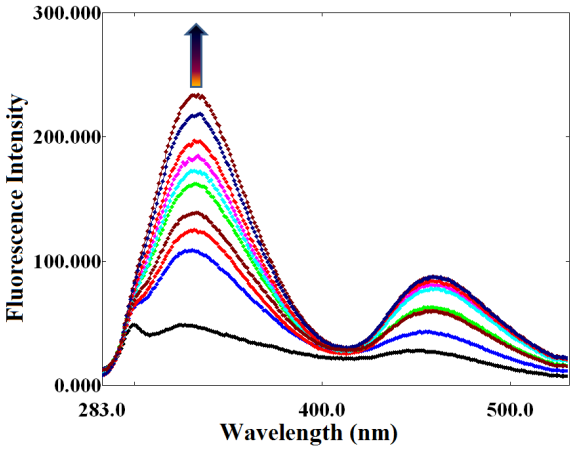

Fig. 6

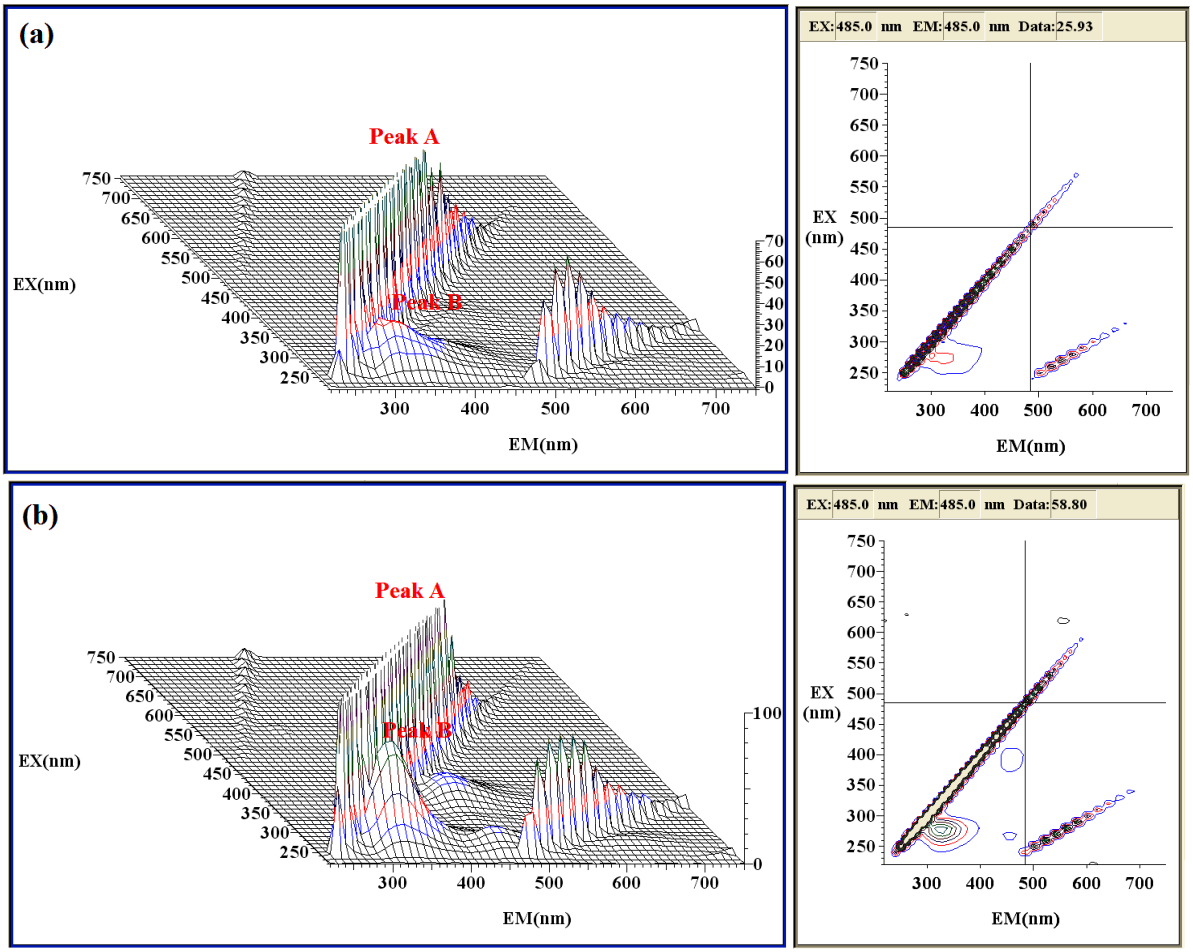

Fig. 7

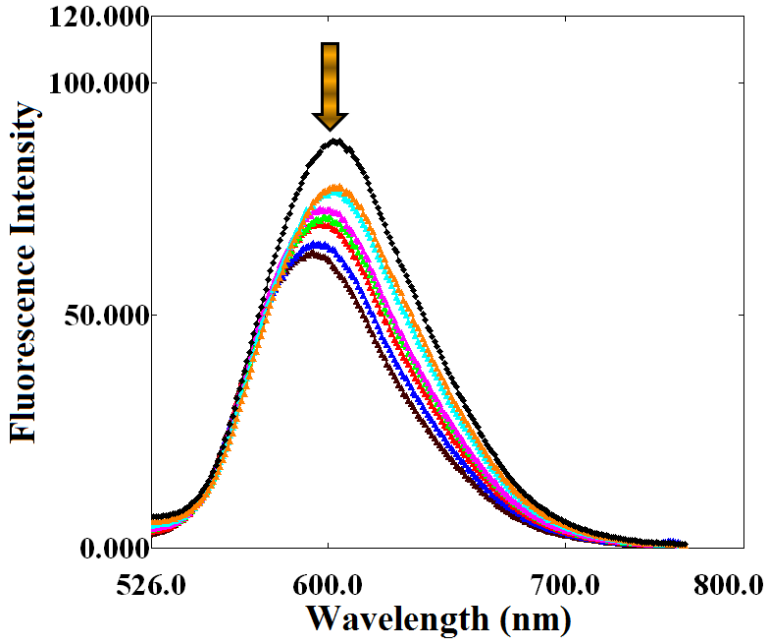

Fig. 8

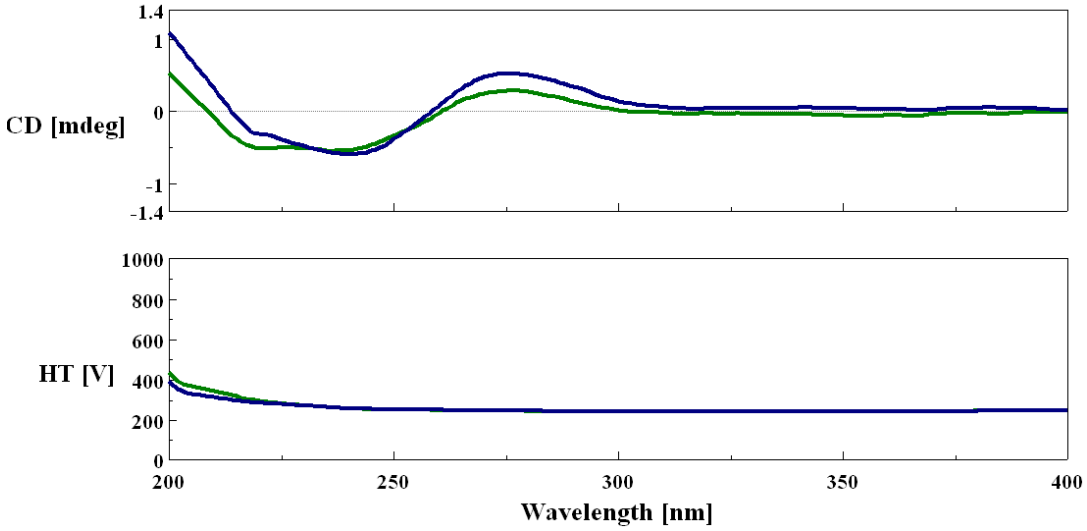

Fig. 9

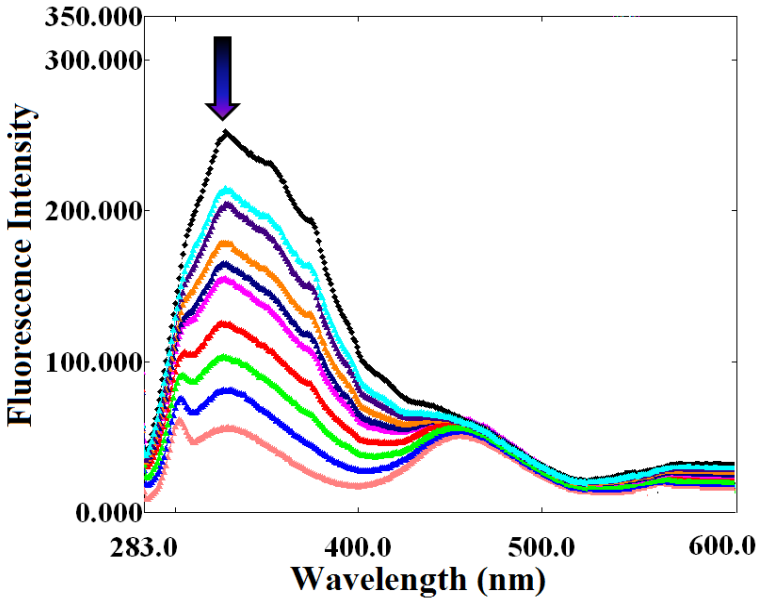

Fig. 10

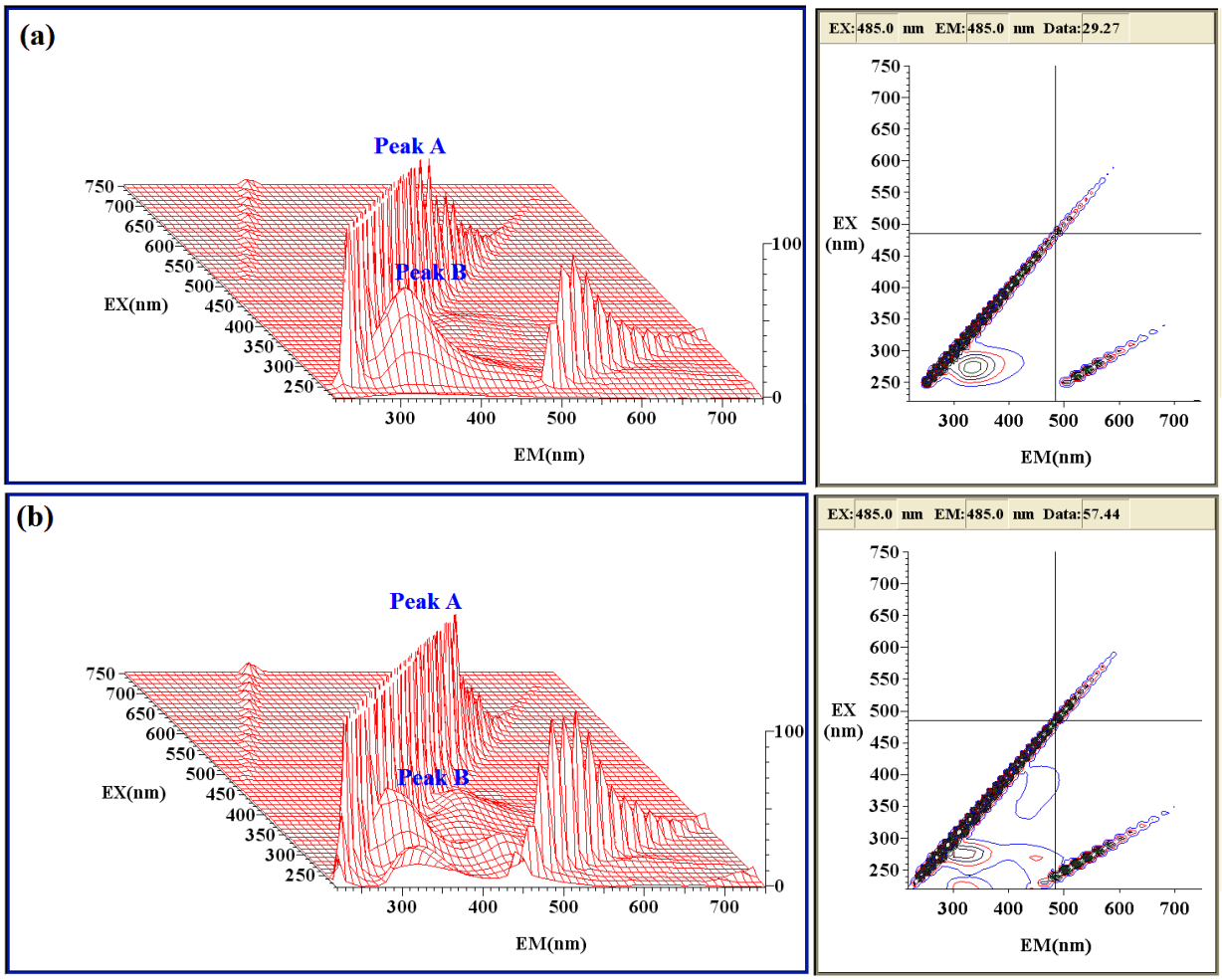

Fig. 11

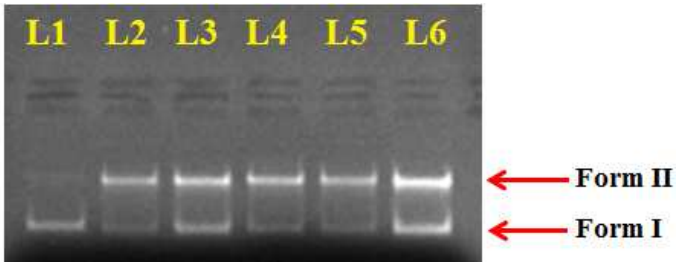

Fig. 12

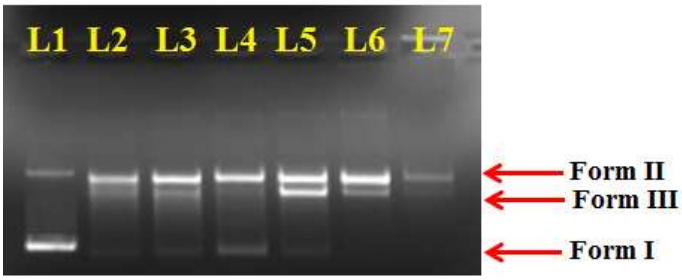

Fig. 13

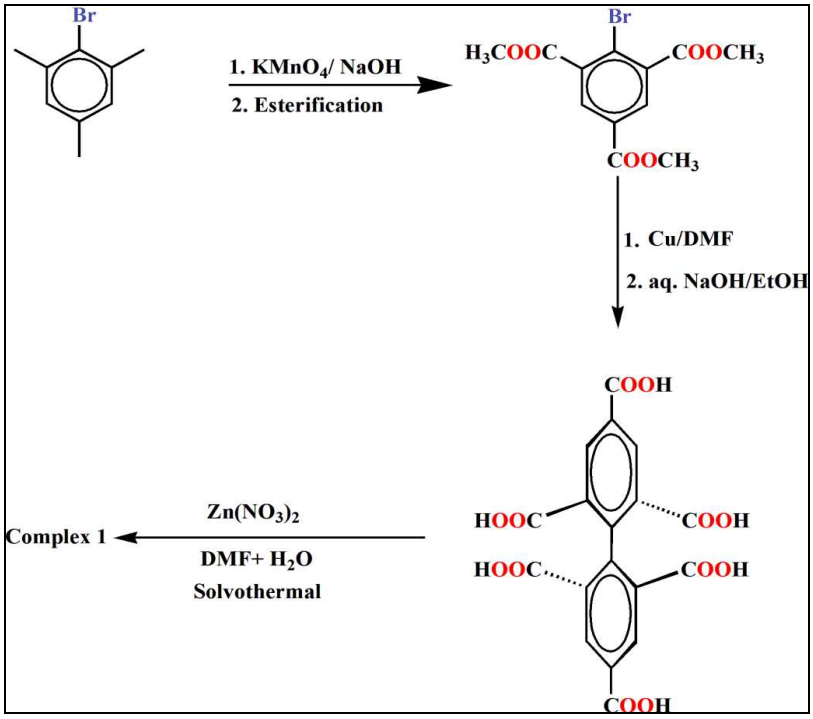

Scheme 1

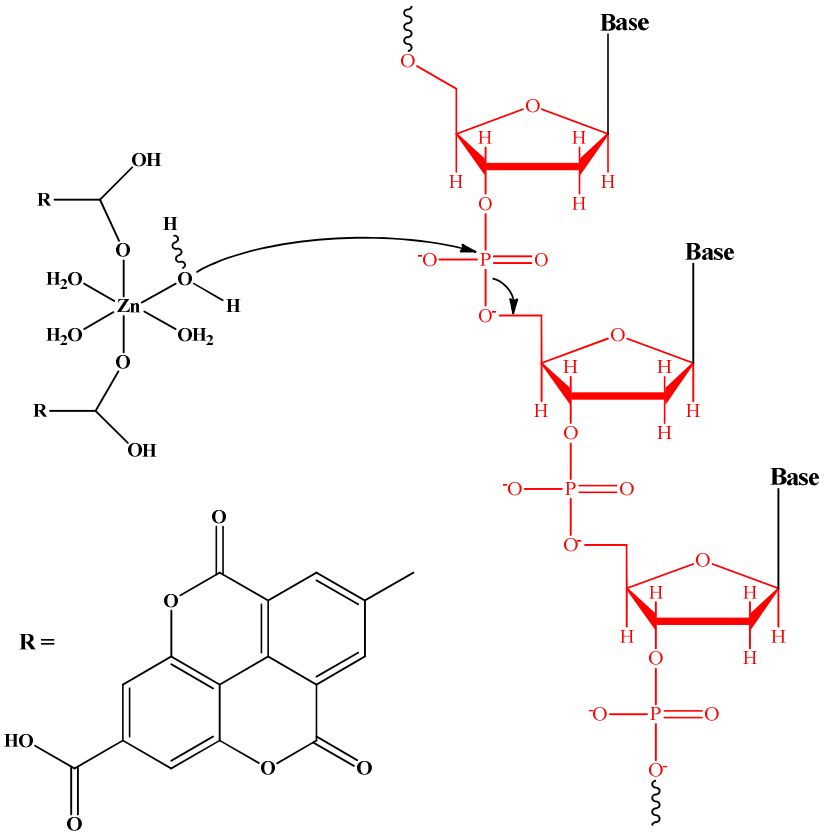

Scheme 2